RESEARCH ARTICLE | APRIL 07 2015

Cattaneo-Christov heat flux model for rotating flow and heat transfer of upper-convected Maxwell fluid

Meraj Mustafa

AIP Advances 5, 047109 (2015)
https://doi.org/10.1063/1.4917306

AIP ADVANCES **5**, 047109 (2015)

Cattaneo-Christov heat flux model for rotating flow and heat transfer of upper-convected Maxwell fluid

Meraj Mustafa[a]
School of Natural Sciences (SNS), National University of Sciences and Technology (NUST), Islamabad 44000, Pakistan

(Received 24 February 2015; accepted 30 March 2015; published online 7 April 2015)

In this paper Cattaneo-Christov heat flux model is used to investigate the rotating flow of viscoelastic fluid bounded by a stretching surface. This model is a modified version of the classical Fourier's law that takes into account the interesting aspect of thermal relaxation time. The boundary layer equations are first modeled and then reduced to self-similar forms via similarity approach. Both analytical and numerical solutions are obtained and found in excellent agreement. Our computations reveal that velocity is inversely proportional to the viscoelastic fluid parameter. Further fluid temperature has inverse relationship with the relaxation time for heat flux and with the Prandtl number. Present consideration even in the case of Newtonian fluid does not yet exist in the literature. [http://dx.doi.org/10.1063/1.4917306]

I. INTRODUCTION

The classical Fourier's heat conduction law[1] has been the most successful model for the description of heat transfer mechanism in various pertinent situations. Despite this fact it has a major limitation that it yields a parabolic energy equation for the temperature field and hence it contradicts with the principle of causality. Cattaneo,[2] in his famous paper, suggested a successful alteration of the Fourier's model by incorporating an important feature of thermal relaxation time. It is seen that such consideration produces hyperbolic energy equation for temperature field and it allows for the transportation of heat through the propagation of thermal waves having finite speed. Such kind of heat transportation has exciting practical applications that span from nanofluid flows to the modeling of skin burn injury (see Tibullo and Zampoli[3] and refs. therein). It may also be noted that there are several materials for which thermal relaxation time is large such as NaHCO3 (29s), biological tissues (1-100s), sand (21s) and many others. Christov[4] replaced the time derivative in Maxwell-Cattaneo's model with the Oldroyd's upper-convected derivative in order to preserve the material-invariant formulation. This model is recognized in the literature as Cattaneo-Christov heat flux model. Ciarletta and Straughan[5] proved the uniqueness of the solutions for the Cattaneo-Christov equations. Straughan[6] studied the natural convection in horizontal layer of incompressible Newtonian fluid. Recently Han *et al.*[7] studied the slip flow and heat transfer in Maxwell fluid through Cattaneo-Christov model. They solved the governing problem analytically by homotopy analysis method (HAM). They also validated their solutions with the numerical solutions via finite difference approach.

Present paper aims to explore the characteristics of Cattaneo-Christov heat conduction in rotating flow of upper-convected Maxwell (UCM) fluid. The Maxwell fluid model has received remarkable attention of the researchers due to its simplicity. It can address the behavior of fluid relaxation time on the boundary layer. Some interesting flow problems involving Maxwell fluid can be found in Refs. 8–16 The arising coupled non-linear boundary value problem is treated both analytically and numerically. Highly accurate analytic solutions are obtained by powerful homotopy

[a]Corresponding author Tel.: + 92 51 90855596. E-mail address: meraj_mm@hotmail.com (M. Mustafa)

analysis method (HAM) suggested by Liao.[17] The numerical solutions are achieved via collocation method. The behavior of involved parameters especially the thermal relaxation time is thoroughly emphasized by graphical illustrations.

II. PROBLEM FORMULATION

Let us consider the flow of upper-convected Maxwell (UCM) fluid bounded by a linearly stretching surface. The fluid is rotating about the $z-$ axis with the angular velocity Ω. The velocity of the sheet is assumed to be $U_w(x) = ax$. Let T_w be the constant temperature at the sheet whereas T_∞ is the ambient value of the temperature such that $T_w > T_\infty$. Using the velocity field $\mathbf{V} = [u(x,y,z), v(x,y,z), w(x,y,z)]$ and the temperature field $T = T(x,y,z)$ the boundary layer equations for flow and heat transfer of UCM fluid can be expressed as below.

$$\frac{\partial u}{\partial x} + \frac{\partial v}{\partial y} + \frac{\partial w}{\partial z} = 0, \tag{1}$$

$$u\frac{\partial u}{\partial x} + v\frac{\partial u}{\partial y} + w\frac{\partial u}{\partial z} - 2\Omega v = \nu\frac{\partial^2 u}{\partial z^2} - \lambda_1\left(\begin{array}{l} u^2\dfrac{\partial^2 u}{\partial x^2} + v^2\dfrac{\partial^2 u}{\partial y^2} + w^2\dfrac{\partial^2 u}{\partial z^2} \\ +2uv\dfrac{\partial^2 u}{\partial x\partial y} + 2vw\dfrac{\partial^2 u}{\partial y\partial z} + 2uw\dfrac{\partial^2 u}{\partial x\partial z}\end{array}\right), \tag{2}$$

$$u\frac{\partial v}{\partial x} + v\frac{\partial v}{\partial y} + w\frac{\partial v}{\partial z} + 2\Omega u = \nu\frac{\partial^2 v}{\partial z^2} - \lambda_1\left(\begin{array}{l} u^2\dfrac{\partial^2 v}{\partial x^2} + v^2\dfrac{\partial^2 v}{\partial y^2} + w^2\dfrac{\partial^2 v}{\partial z^2} \\ +2uv\dfrac{\partial^2 v}{\partial x\partial y} + 2vw\dfrac{\partial^2 v}{\partial y\partial z} + 2uw\dfrac{\partial^2 v}{\partial x\partial z}\end{array}\right), \tag{3}$$

$$\rho c_p\left(u\frac{\partial T}{\partial x} + v\frac{\partial T}{\partial y} + w\frac{\partial T}{\partial z}\right) = -\nabla\cdot\mathbf{q}, \tag{4}$$

where u, v and w are the velocity components along the $x-, y-$ and z-directions respectively, ν is the kinematic viscosity, T is the fluid temperature, c_p is the specific heat, ρ is the fluid density, λ_1 is the fluid relaxation time and $\mathbf{q}$ is the heat flux which satisfies the following relationship.[3]

$$\mathbf{q} + \lambda_2\left(\frac{\partial \mathbf{q}}{\partial t} + \mathbf{V}.\nabla\mathbf{q} - \mathbf{q}.\nabla\mathbf{V} + (\nabla.\mathbf{V})\mathbf{q}\right) = -k\nabla T, \tag{5}$$

in which λ_2 is the thermal relaxation time and k is the thermal conductivity of the fluid. Following Cristov,[3] we eliminate $\mathbf{q}$ from Eqs. (4) and (5) to obtain the following:

$$u\frac{\partial T}{\partial x} + v\frac{\partial T}{\partial y} + w\frac{\partial T}{\partial z} = \frac{k}{\rho c_p}\frac{\partial^2 T}{\partial z^2} - \lambda_2\left[\begin{array}{l} u^2\dfrac{\partial^2 T}{\partial x^2} + v^2\dfrac{\partial^2 T}{\partial y^2} + w^2\dfrac{\partial^2 T}{\partial z^2} + 2uv\dfrac{\partial^2 T}{\partial x\partial y} + 2vw\dfrac{\partial^2 T}{\partial y\partial z} \\ +2uw\dfrac{\partial^2 T}{\partial x\partial z} + \left(u\dfrac{\partial u}{\partial x} + v\dfrac{\partial u}{\partial y} + w\dfrac{\partial u}{\partial z}\right)\dfrac{\partial T}{\partial x} \\ + \left(u\dfrac{\partial v}{\partial x} + v\dfrac{\partial v}{\partial y} + w\dfrac{\partial v}{\partial z}\right)\dfrac{\partial T}{\partial y} + \left(u\dfrac{\partial w}{\partial x} + v\dfrac{\partial w}{\partial y} + w\dfrac{\partial w}{\partial z}\right)\dfrac{\partial T}{\partial z}\end{array}\right]. \tag{6}$$

The boundary conditions in the present problem are:

$$\begin{array}{c} u = ax, \quad v = 0, \quad w = 0, \quad T = T_w \quad \text{at} \quad z = 0, \\ u \to 0, \quad v \to 0, \quad T \to T_\infty \quad \text{as} \quad z \to \infty. \end{array} \tag{7}$$

Invoking the following similarity transformations

$$\eta = \sqrt{\frac{a}{\nu}}z, \qquad u = axf'(\eta), \qquad v = axg(\eta), \qquad w = -\sqrt{a\nu}f(\eta), \qquad \theta = \frac{T - T_\infty}{T_w - T_\infty}, \tag{8}$$

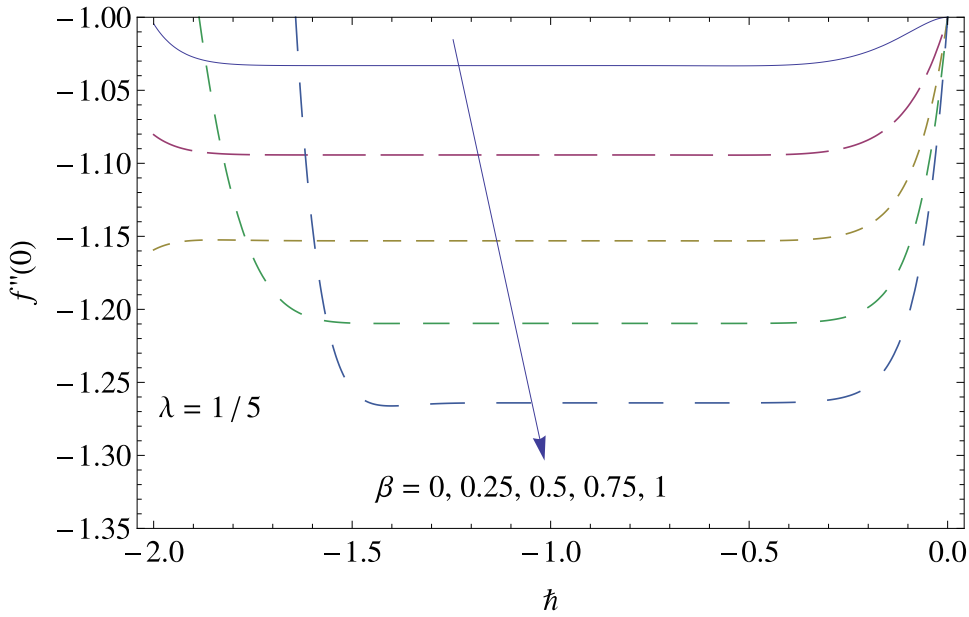

FIG. 1. $\hbar$– curves of $f''(0)$ at 15th-order of approximations.

Eq. (1) is identically satisfied and Eqs. (2), (3), (6), and (7) take the following forms:

$$f''' - f'^2 + ff'' + 2\lambda g + \beta\left[2ff'f'' - f^2 f'''\right] = 0, \tag{9}$$

$$g'' + fg' - f'g - 2\lambda f' + \beta\left[2ff'g' - f^2 g''\right] = 0, \tag{10}$$

$$\frac{1}{Pr}\theta'' + f\theta' - \gamma\left[ff'\theta' + f^2\theta''\right] = 0, \tag{11}$$

$$\begin{aligned} &f(0) = g(0) = 0, \qquad f'(0) = 1, \qquad \theta(0) = 1, \\ &f'(\infty) \to 0, \qquad g(\infty) \to 0, \qquad \theta(\infty) \to 0, \end{aligned} \tag{12}$$

where $\lambda = \Omega/a$ is the rotation parameter, $\beta = \lambda_1 a$ is the Deborah number, $\gamma = \lambda_2 a$ is the non-dimensional thermal relaxation time and $\mathrm{Pr} = \mu c_p/k$ is the Prandtl number.

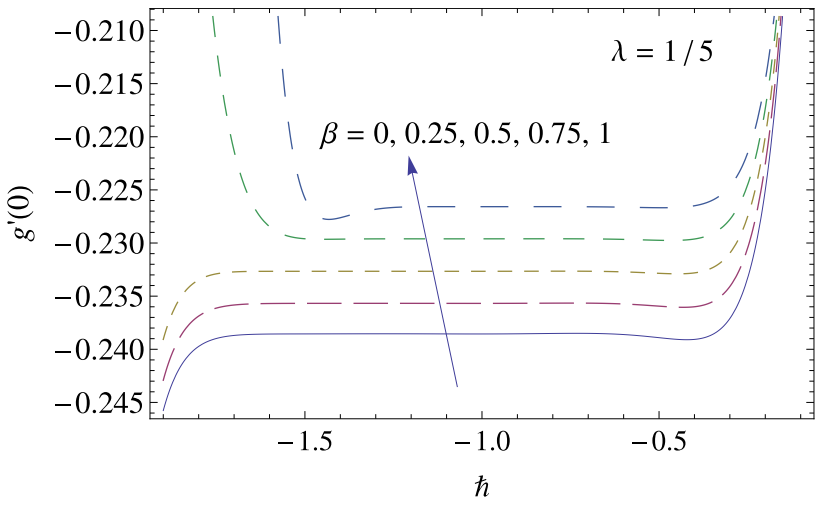

FIG. 2. $\hbar$– curves of $g'(0)$ at 15th-order of approximations.

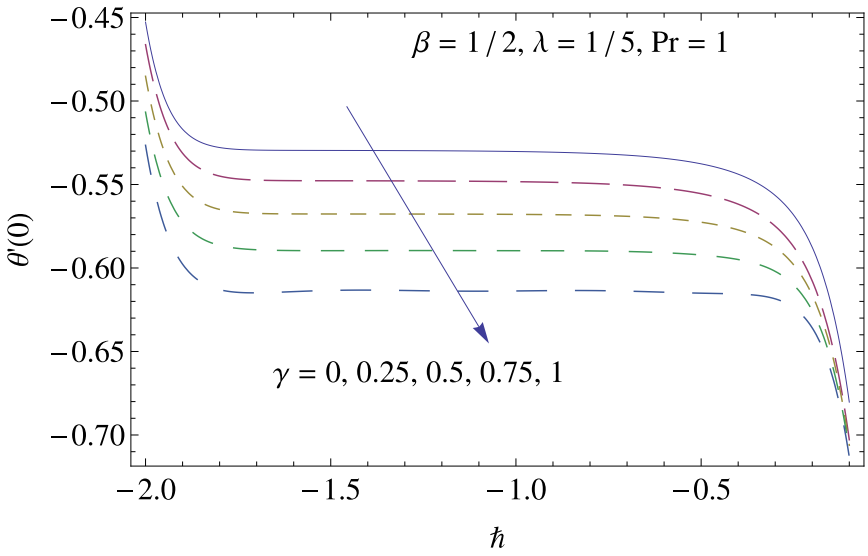

FIG. 3. $\hbar$– curves of $\theta'(0)$ at 15$^{\text{th}}$-order of approximations.

III. ANALYTIC SOLUTIONS BY HAM

The solution of coupled equations (9)-(11) with the boundary conditions (12) is obtained in series form by a powerful homotopy analysis method (HAM). Based on the so called *rule of solution expression* and the conditions (12) it seems appropriate to choose the following initial guesses for functions f, g and θ

$$f_0(\eta) = 1 - \exp(-\eta), \qquad g_0(\eta) = 0, \qquad \theta_0(\eta) = \exp(-\eta), \tag{13}$$

and the auxiliary linear operators are selected as below:

$$\mathbf{L}_f \equiv \frac{d^3}{d\eta^3} - \frac{d}{d\eta}, \qquad \mathbf{L}_g \equiv \frac{d^2}{d\eta^2} - 1, \qquad \mathbf{L}_\theta \equiv \frac{d^2}{d\eta^2} - 1. \tag{14}$$

Let $q \in [0, 1]$ be an embedding parameter and $\hbar$ be the non-zero auxiliary parameter. The generalized homotopic equations for Eqs. (9)-(12) can be constructed in the following forms:

$$(1-q)\mathbf{L}_f[F(\eta, q) - f_0(\eta)] = q\hbar\mathbf{N}_f\left[F(\eta, q), G(\eta, q)\right], \tag{15}$$

$$(1-q)\mathbf{L}_g[G(\eta, q) - g_0(\eta)] = q\hbar\mathbf{N}_g\left[F(\eta, q), G(\eta, q)\right], \tag{16}$$

$$(1-q)\mathbf{L}_\theta[\Theta(\eta, q) - \theta_0(\eta)] = q\hbar\mathbf{N}_\theta\left[F(\eta, q), \Theta(\eta, q)\right], \tag{17}$$

TABLE I. Comparison of 25$^{\text{th}}$-order HAM solutions for $f''(0)$ and $g'(0)$ with the numerical solutions at different values of β.

	$f''(0)$		$g'(0)$	
β	HAM	Numerical	HAM	Numerical
0	−1.033105	−1.033105	−0.238547	−0.238546
0.2	−1.082246	−1.082246	−0.236267	−0.236267
0.4	−1.129840	−1.129839	−0.233876	−0.233875
0.6	−1.175951	−1.175950	−0.231438	−0.231436
0.8	−1.220659	−1.220659	−0.228997	−0.228997
1.0	−1.264050	−1.264040	−0.226580	−0.226580

TABLE II. Comparison of 35th-order HAM solutions for $\theta'(0)$ with the numerical solutions at different values of γ.

γ		**0**	**0.2**	**0.4**	**0.6**	**0.8**
$\theta'(0)$	HAM	−0.529525	−0.543940	−0.559451	−0.576171	−0.594210
	Numerical	−0.529525	−0.543940	−0.559451	−0.576171	−0.594211

$$F(\eta,q)|_{\eta=0}=0,\qquad \left.\frac{\partial F(\eta,q)}{\partial\eta}\right|_{\eta=0}=1,\qquad G(\eta,q)|_{\eta=0}=0,\qquad \Theta(\eta,q)|_{\eta=0}=0,$$
$$\left.\frac{\partial F(\eta;q)}{\partial\eta}\right|_{\eta\to+\infty}=0,\qquad G(\eta,q)|_{\eta\to+\infty}=0,\qquad \Theta(\eta,q)|_{\eta\to+\infty}=0, \tag{18}$$

in which the non-linear operators $\mathbf{N}_f$, $\mathbf{N}_\theta$ and $\mathbf{N}_\phi$ are as under:

$$\mathbf{N}_f[F(\eta,q),G(\eta,q)]=\frac{\partial^3F(\eta,q)}{\partial\eta^3}+F(\eta,q)\frac{\partial^2F(\eta,q)}{\partial\eta^2}-\left(\frac{\partial F(\eta,q)}{\partial\eta}\right)^2+2\lambda G(\eta,q)$$
$$+\beta\left(F(\eta,q)\frac{\partial F(\eta,q)}{\partial\eta}\frac{\partial^2F(\eta,q)}{\partial\eta^2}-(F(\eta,q))^2\frac{\partial^3F(\eta,q)}{\partial\eta^3}\right), \tag{19}$$

$$\mathbf{N}_g[F(\eta,q),G(\eta,q)]=\frac{\partial^2G(\eta,q)}{\partial\eta^2}+F(\eta,q)\frac{\partial G(\eta,q)}{\partial\eta}-\frac{\partial F(\eta,q)}{\partial\eta}G(\eta,q)-2\lambda\frac{\partial F(\eta,q)}{\partial\eta}$$
$$+\beta\left(F(\eta,q)\frac{\partial F(\eta,q)}{\partial\eta}\frac{\partial G(\eta,q)}{\partial\eta}-(F(\eta,q))^2\frac{\partial^2G(\eta,q)}{\partial\eta^2}\right), \tag{20}$$

$$\mathbf{N}_\theta[F(\eta,q),\Theta(\eta,q)]=\frac{1}{\mathrm{Pr}}\frac{\partial^2\Theta(\eta,q)}{\partial\eta^2}+F(\eta,p)\frac{\partial\Theta(\eta,q)}{\partial\eta}$$
$$-\gamma\left[F(\eta,p)\frac{\partial F(\eta,q)}{\partial\eta}\frac{\partial\Theta(\eta,q)}{\partial\eta}+(F(\eta,p))^2\frac{\partial^2\Theta(\eta,q)}{\partial\eta^2}\right]. \tag{21}$$

$$F(\eta,q)|_{\eta=0}=0,\qquad \left.\frac{\partial F(\eta,q)}{\partial\eta}\right|_{\eta=0}=1,\qquad G(\eta,q)|_{\eta=0}=0,\qquad \Theta(\eta,q)|_{\eta=0}=0,$$
$$\left.\frac{\partial F(\eta;q)}{\partial\eta}\right|_{\eta\to+\infty}=0,\qquad G(\eta,q)|_{\eta\to+\infty}=0,\qquad \Theta(\eta,q)|_{\eta\to+\infty}=0, \tag{22}$$

Now expanding the functions $F(\eta,q)$, $G(\eta,q)$ and $\Theta(\eta,q)$ by Taylor series about $q=0$, one obtains

$$F(\eta,q)=f_0(\eta)+\sum_{m=1}^{\infty}f_m(\eta)q^m;\quad f_m(\eta)=\left.\frac{1}{m!}\frac{\partial^mF(\eta,q)}{\partial q^m}\right|_{q=0}, \tag{23}$$

$$G(\eta,q)=g_0(\eta)+\sum_{m=1}^{\infty}g_m(\eta)q^m;\quad g_m(\eta)=\left.\frac{1}{m!}\frac{\partial^mG(\eta,q)}{\partial q^m}\right|_{q=0}, \tag{24}$$

$$\Theta(\eta,q)=\theta_0(\eta)+\sum_{m=1}^{\infty}\theta_m(\eta)q^m;\quad \theta_m(\eta)=\left.\frac{1}{m!}\frac{\partial^m\Theta(\eta,q)}{\partial q^m}\right|_{q=0}. \tag{25}$$

It is clear that the above equations give the final solution at $q=1$. The functions f_m, g_m and θ_m can be easily computed from the deformation equations corresponding to Eqs. (9)-(12). The mth-order deformation problems are obtained as

$$\mathbf{L}_f[f_m(\eta)-\chi_mf_{m-1}(\eta)]=\hbar\mathbf{R}_m^f(\eta), \tag{26}$$
$$\mathbf{L}_g[g_m(\eta)-\chi_mg_{m-1}(\eta)]=\hbar\mathbf{R}_m^g(\eta), \tag{27}$$
$$\mathbf{L}_\theta[\theta_m(\eta)-\chi_m\theta_{m-1}(\eta)]=\hbar\mathbf{R}_m^\theta(\eta), \tag{28}$$

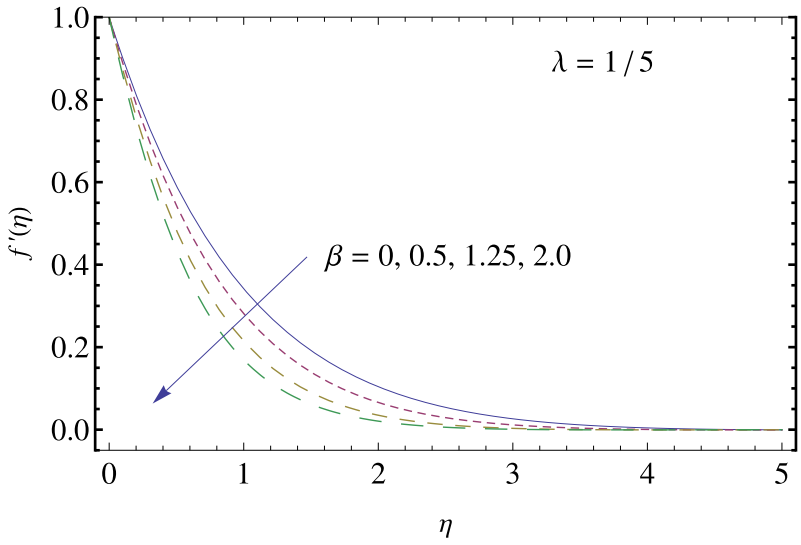

FIG. 4. Influence of β on f'.

$$f_m(0) = 0, \qquad \left.\frac{df_m(\eta)}{d\eta}\right|_{\eta=0} = 0, \qquad g_m(0) = 0, \qquad \theta_m(0) = 0,$$
$$\left.\frac{\partial f_m(\eta)}{\partial \eta}\right|_{\eta\to+\infty} = 0, \qquad g_m(\infty) = 0, \qquad \theta_m(\infty) = 0, \tag{29}$$

where the functions $\mathbf{R}_m^f(\eta)$, $\mathbf{R}_m^g(\eta)$ and $\mathbf{R}_m^\theta(\eta)$ have the following forms

$$\mathbf{R}_m^f(\eta) = \frac{\partial^3 f_{m-1}}{\partial\eta^3} + 2\lambda g_{m-1} + \beta\sum_{k=0}^{m-1}\left[f_{m-1-k}\sum_{l=0}^{k}\frac{\partial f_{k-l}}{\partial\eta}\frac{\partial^2 f_l}{\partial\eta^2} - f_{m-1-k}\sum_{l=0}^{k} f_{k-l}\frac{\partial^3 f_l}{\partial\eta^3}\right]$$
$$+\sum_{k=0}^{m-1}\left[f_{m-1-k}\frac{\partial^2 f_k}{\partial\eta^2} - \frac{\partial f_{m-1-k}}{\partial\eta}\frac{\partial f_k}{\partial\eta}\right], \tag{30}$$

$$\mathbf{R}_m^g(\eta) = \frac{\partial^2 g_{m-1}}{\partial\eta^2} - 2\lambda\frac{\partial f_{m-1}}{\partial\eta} + \beta\sum_{k=0}^{m-1}\left[f_{m-1-k}\sum_{l=0}^{k}\frac{\partial f_{k-l}}{\partial\eta}\frac{\partial g_k}{\partial\eta} - f_{m-1-k}\sum_{l=0}^{k} f_{k-l}\frac{\partial^2 g_l}{\partial\eta^2}\right]$$
$$+\sum_{k=0}^{m-1}\left[f_{m-1-k}\frac{\partial g_k}{\partial\eta} - \frac{\partial f_{m-1-k}}{\partial\eta}g_k\right], \tag{31}$$

$$\mathbf{R}_m^\theta(\eta) = \frac{1}{\mathrm{Pr}}\frac{\partial^2\theta_{m-1}}{\partial\eta^2} + \sum_{k=0}^{m-1}\left[f_{m-1-k}\frac{\partial\theta_k}{\partial\eta} - \gamma\left(f_{m-1-k}\sum_{l=0}^{k}\frac{\partial f_{k-l}}{\partial\eta}\frac{\partial\theta_k}{\partial\eta} + f_{m-1-k}\sum_{l=0}^{k} f_{k-l}\frac{\partial^2\theta_l}{\partial\eta^2}\right)\right], \tag{32}$$

$$\chi_m = \begin{cases} 0, & m \le 1, \\ 1, & m > 1. \end{cases} \tag{33}$$

Thus the non-linear differential system (9)-(12) is now reduced to several linear differential equations given in Eqs. (26)-(33) which can be solved exactly through the computational software such as *Mathematica* or *Maple* for $m = 1, 2, 3, \ldots$.

A. Convergence of the series solutions

The convergence of the series (23)-(25) depends on the choice of the auxiliary parameter $\hbar$. To select proper $\hbar$, we plot the so called $\hbar-$ curves of velocity and temperature gradients at 15^{th}-order

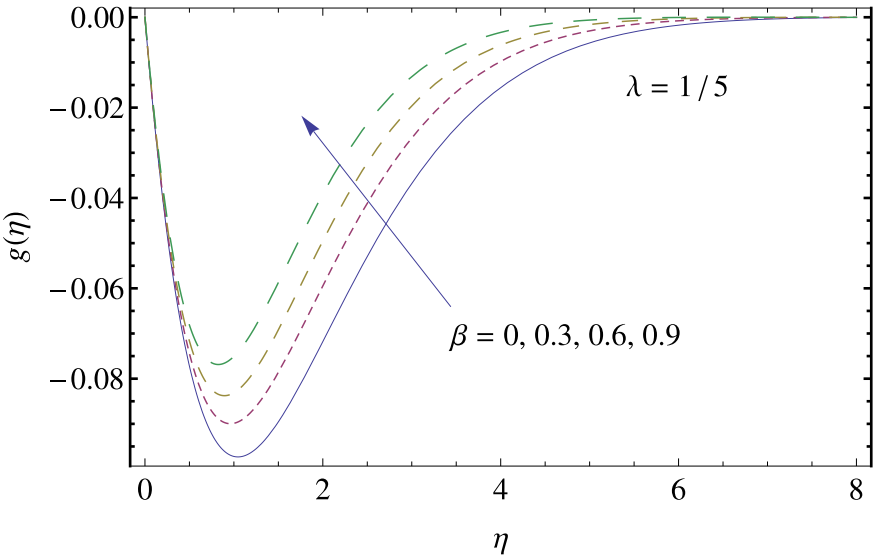

FIG. 5. Influence of β on g.

of approximations (see Figs. 1, 2, and 3). As suggested by Liao,[17] the valid region for $\hbar$ can be obtained through the line segment parallel to $\hbar-$ axis. For example when $\beta = 1/2, \lambda = 1/5, \mathrm{Pr} = 1$ and $\gamma = 0.5$ the intervals of convergence for f, g and θ are $[-1.8, -0.5]$, $[-1.6, -0.6]$ and $[-1.3, -0.9]$ respectively.

IV. RESULTS AND DISCUSSION

In addition to the analytic solutions, the boundary value problem (9)-(12) has also been solved numerically by collocation method through the built in routine *bvp4c* of the software *Matlab*. First of all we compare the 25$^{\text{th}}$-order HAM solutions for $f''(0)$ and $g'(0)$ with the numerical solutions in Table I. The results appear to be almost identical by both the methods for all the considered values of the Deborah number β. It is observed that $f''(0)$, which measures the stress at the wall, increases when β is incremented. Table II includes the comparison of 35$^{\text{th}}$-order HAM solution for $\theta'(0)$ with the numerical solutions at different values of thermal relaxation time γ and this comparison is found

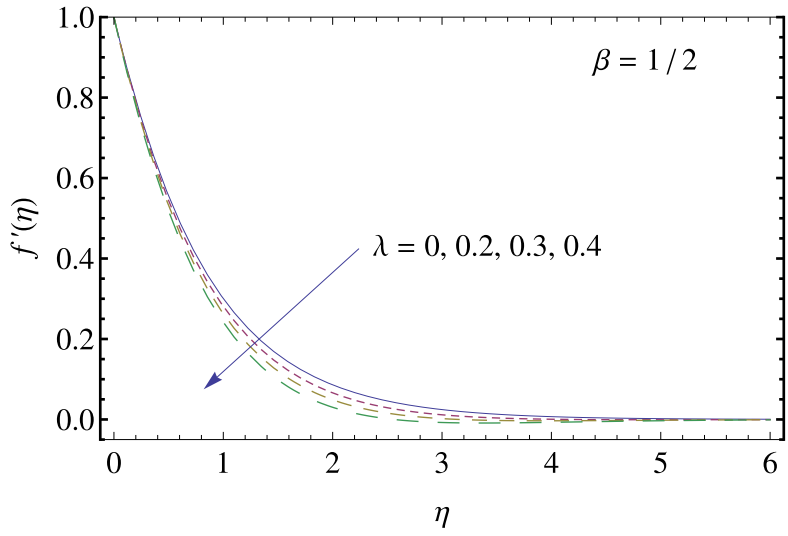

FIG. 6. Influence of λ on f'.

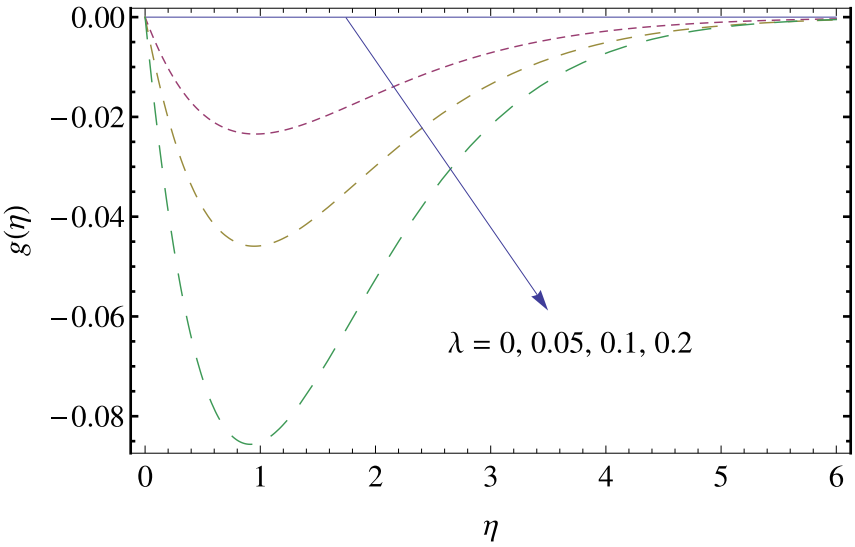

FIG. 7. Influence of λ on g.

to be very good. This gives us confidence that present homotopy solutions are highly accurate for both large/small values of the involved parameters.

In Fig. 4, we plot the velocity field f' for different values of Deborah number β. The velocity in the horizontal direction decreases with an increase in β. From the physical point of view, the larger values of β indicates stronger viscous force which resists the flow and hence velocity decreases. We notice that profiles are tilted towards the boundary when β is increased. This indicates that boundary layer thickness is a decreasing function of β. Fig. 5 reveals that velocity field g has a parabolic distribution. It is clear that magnitude of g is inversely proportional to β. Thus velocity in the vertical direction would be lesser for larger Deborah number fluid. The influence of rotation parameter λ on the velocity fields can be described from Figs. 6 and 7. The velocity in both $x-$ and $y-$ directions appears to decrease with an increase in the angular velocity about the $z-$ axis.

The impact of non-dimensional heat flux relaxation time γ on temperature can be explained through Fig. 8. It is clear that both temperature θ and the thermal boundary layer thickness are

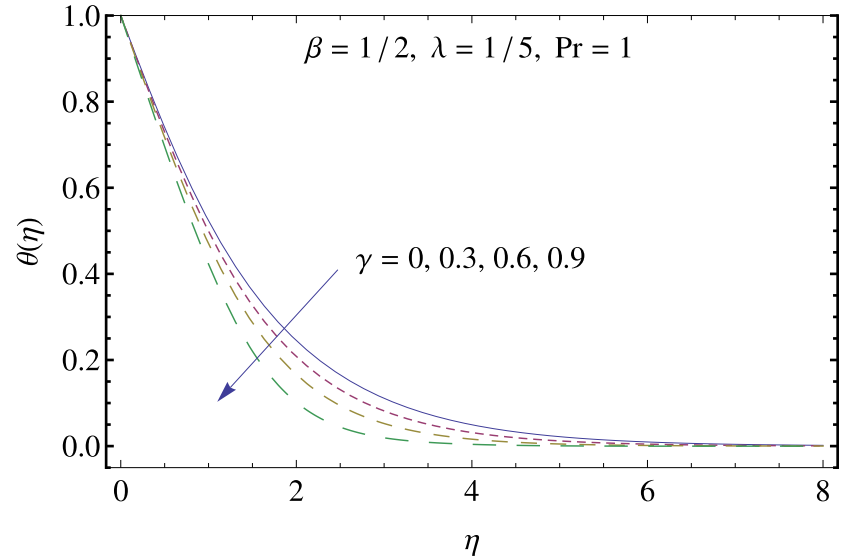

FIG. 8. Influence of γ on θ.

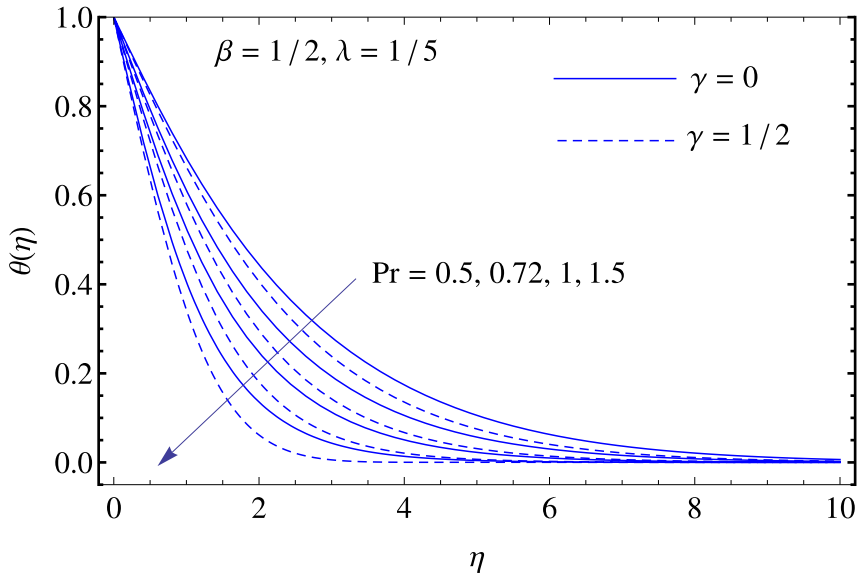

FIG. 9. Influence of Pr on θ.

inversely proportional to the thermal relaxation time λ_2. This outcome agrees with that of Han *et al.*[7] Thus it can be concluded that temperature in Cattaneo-Christov heat conduction model is smaller than that in Fourier's model.

Fig. 9 compares the temperature distribution in Fourier and Cattaneo-Christov heat flux models. From the qualitative point of view the behavior of Pr in both the cases is similar i.e temperature decreases when Pr is increased. It can be seen that penetration depth of θ is much bigger at Pr = 0.5 when compared with Pr = 1.5. An increase in Pr corresponds to a decrease in thermal diffusivity and hence thinner thermal boundary layer exists for larger Prandtl number fluid. The wall temperature gradient $-\theta'(0)$ is plotted against the Prandtl number Pr for different values of non-dimensional thermal relaxation time γ in Fig. 10. We found that $\theta'(0)$ linearly increases with an increase in Pr. However it is a decreasing function of γ.

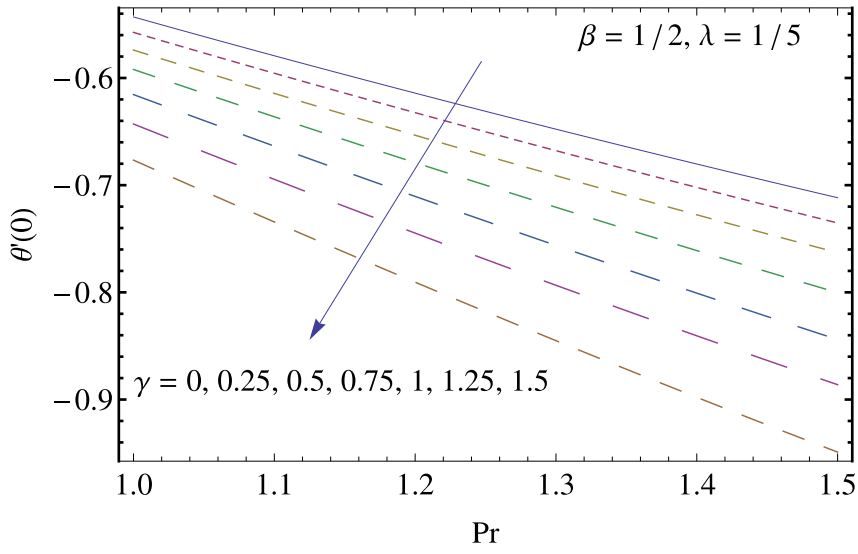

FIG. 10. Wall temperature gradient for different values of γ.

V. CONCLUSIONS

Rotating flow of upper-convected Maxwell fluid is examined with the consideration of Cattaneo-Christov heat flux model that accounts for the effects of thermal relaxation time. Highly accurate solutions of the strongly non-linear differential system are obtained by both analytical and numerical methods. The main observations of this work are summarized as below:

(1) The HAM based series solutions are found in agreement with the numerical solutions.
(2) Velocity in both the $x-$ and $y-$ directions is found to decrease upon increasing the Deborah number β.
(3) Temperature θ and thermal boundary thickness are inversely proportional to the thermal relaxation time.
(4) The influence of embedded parameters is found to be qualitatively similar in both Fourier and Cattaneo-Christov heat conduction models.
(5) Present analysis for the Newtonian fluid case can be retrieved as special case of this work by selecting $\beta = 0$.

[1] J. B. J. Fourier, *Théorie Analytique De La Chaleur* (Paris, 1822).
[2] C. Cattaneo, "Sulla conduzionedelcalore," AttiSemin. Mat. Fis. Univ. Modena Reggio Emilia **3**, 83–101 (1948).
[3] V. Tibullo and V. Zampoli, "A uniqueness result for the Cattaneo–Christov heat conduction model applied to incompressible fluids," Mech. Res. Commun. **38**, 77–79 (2011).
[4] C. I. Christov, "On frame indifferent formulation of the Maxwell–Cattaneo model of finite-speed heat conduction," Mech. Res. Commun. **36**, 481–486 (2009).
[5] B. Straughan, "Thermal convection with the Cattaneo–Christov model," Int. J. Heat Mass Transf. **53**, 95–98 (2010).
[6] M. Ciarletta and B. Straughan, "Uniqueness and structural stability for the Cattaneo–Christov equations," Mech. Res. Commun. **37**, 445–447 (2010).
[7] S. Han, L. Zheng, C. Li, and X. Zhang, "Coupled flow and heat transfer in viscoelastic fluid with Cattaneo–Christov heat flux model," Appl. Math. Lett. **38**, 87–93 (2014).
[8] C. Fetecau, M. Jamil, C. Fetecau, and I. Siddiqui, "A note on the second problem of Stokes for Maxwell fluids," Int. J. Non-Linear Mech. **44**, 1085-1090 (2009).
[9] M. Kumari and G. Nath, "Steady mixed convection stagnation-point flow of upper convected Maxwell fluids with magnetic field," Int. J. Non-Linear Mech. **44**, 1048-1055 (2009).
[10] T. Hayat, M. Mustafa, and S. Mesloub, "Mixed convection boundary layer flow over a stretching surface filled with a Maxwell fluid in presence of Soret and Dufour effects," Z. Naturforsch. **65a**, 401-410 (2010).
[11] K. L. Hsiao, "MHD mixed convection for viscoelastic fluid past a porous wedge," Int. J. Non-Linear Mech. **46**, 1-8 (2011).
[12] T. Hayat, M. Mustafa, S. A. Shehzad, and S. Obaidat, "Melting heat transfer in the stagnation-point flow of an upper-convected Maxwell (UCM) fluid past a stretching sheet," Int. J. Numer. Meth. Fluids **68**, 233-243 (2012).
[13] S. Shateyi, "A new numerical approach to MHD flow of a Maxwell fluid past a vertical stretching sheet in the presence of thermophoresis and chemical reaction," Bound. Val. Prob. **196**, 1687-2770 (2013).
[14] K. L. Hsiao, "Conjugate heat transfer for mixed convection and Maxwell fluid on a stagnation point," Arab. J. Sci. Eng. **39**, 4325-4332 (2014).
[15] A. Mushtaq, M. Mustafa, T. Hayat, and A. Alsaedi, "Effect of thermal radiation on the stagnation-point flow of upper-convected Maxwell fluid over a stretching sheet," J. Aerosp. Engg. **27**, 04014015 (2014).
[16] M. Mustafa, J. A. Khan, T. Hayat, and A. Alsaedi, "Sakiadis flow of Maxwell fluid considering magnetic field and convective boundary condition," AIP Advances **5** (2015).
[17] S. Liao, "Notes on the homotopy analysis method: Some definitions and theorems," Commun. Nonlinear Sci. Numer. Simul. **14**, 983-997 (2009).